

Coupling of quantum-dot states via elastic-cotunneling and crossed Andreev reflection in a minimal Kitaev chain

Zhi-Hai Liu,^{1,*} Chuanchang Zeng,^{1,†} and H. Q. Xu^{2,1,‡}

¹*Beijing Academy of Quantum Information Sciences, Beijing 100193, China*

²*Beijing Key Laboratory of Quantum Devices, Key Laboratory for the Physics and Chemistry of Nanodevices, and School of Electronics, Peking University, Beijing 100871, China*

(Dated: March 14, 2024)

Recently, exciting progress has been made in using the superconducting nanowires coupled to gate-defined quantum dots (QDs) to mimic the Kitaev chain and realize the Majorana-bound states via a poor man's route. The essential ingredient is to balance the interdot elastic-cotunneling (ECT) and crossed Andreev reflection (CAR). As theoretically proposed, this can be mediated by the Andreev bound states (ABSs) formed in the superconducting nanowires. However, most of the gate-tuning asymmetric features observed in experiments can not be captured using the current theoretical models. To address this insufficiency, here, we consider a full model that explicitly includes all the details of both the QD states and the ABSs. Remarkable agreement is found with the recent experimental observations, where our model correctly reveals the gate-tuning asymmetry in ECTs and by which the average QD state energy can also be extracted. In contrast, CARs do not depend on the tuning of QD states. Moreover, armed with the tunability of ECTs and CARs with QD states, we also predict a controllable anisotropic superexchange interaction between electron spins in the two separated QDs.

Introduction—Semiconductor-superconductor hybrid nanostructures have recently attracted intensive attention for the exploration of nontrivial physical phenomena [1–4]. Attributed to strong spin-orbit interactions (SOIs) and large Landé- g factors of narrow-bandgap III-V semiconductors, superconducting nanowires have exhibited as excellent platforms for the studies of the anomalous current-phase relations [5–8], superconducting diode effects [9–12], and Majorana bound states (MBSs) [13–15]. When coupled with the gate-defined quantum dots (QDs), superconducting nanowires can also enable the formation of superconducting spin qubits [16–22] and be exploited to build singlet or triplet Cooper-pair splitters [23–29]. More recently, it has been demonstrated that multiple QDs interconnected by a proximitized semiconductor nanowire can effectively mimic a short Kitaev chain [30–36] and thus construct MBSs in a poor-man's manner [37, 38]. In these burgeoning implementations, the interaction between the separated QDs is found to be mediated by the Andreev bound states (ABSs) residing in the middle proximitized nanowire [26, 29, 37, 38, 41].

Composited as a mix of electron and hole, ABSs simultaneously facilitate the interdot elastic-cotunneling (ECT) and crossed Andreev reflection (CAR) [39, 40]. As revealed by Refs. [32, 37], a fine-tuning reaching the sweet spot is necessarily required to balance ECT and CAR, thereby creating the poor man's MBSs. Additionally, under the interplay between SOI and the externally applied magnetic field, the breaking of spin conservation gives rise to the coexistence of spin-conserved and spin-flipped ECTs and CARs [39]. In effect, the constructions of poor man's MBSs [37, 38], as well as the desired Cooper-pair splitters [26, 29], demand a strict control

of these spin-dependent processes. This highly involves the detailed electron states confined in QDs and tunnel couplings with the ABSs, which, if disregarded, can not ensure a complete picture of the ABS-mediated tunneling processes. For instance, an evident gate-tuning asymmetry is observed for the spin-conserved ECT while absent for the spin-dependent CAR in the recent experiment [39]. More gate-tuning asymmetry appears in the magnetic field for the spin-flipped ECTs therein. These features, however, can not be well-interpreted by the theoretical models to date where the details of QD states, hence the spin-dependent tunneling processes, are not considered [41]. Therefore, it remains a top priority to clarify the effect of the confined states in QDs along with their various modulations on the ABS-mediated CARs and ECTs, as such, to facilitate the studies of rich physics in the systems.

In this Letter, we analyze the ABS-mediated tunneling processes, namely, CARs and ECTs, by constructing a tight-binding (TB) model in close analogy to the experimental setup in Ref. 39 [as schematically shown in Fig. 1(a)]. In such a TB model, all the details of the confined states are explicitly obtainable. Instead of using phenomenal parameters, we obtain the direct tunnel coupling coefficient between QDs and the intermediate ABSs strictly based on the specific localized states of each section. Utilizing the Schrieffer-Wolff transformation, we derive the analytical expressions for the amplitudes of spin-dependent ECTs and CARs that happen between the two QDs. Based on our model, we find that the ECT amplitudes are tightly dependent on the modulation of the on-site energies of the QD states, while the CAR amplitudes remain robust against these modulations. Similar dependencies in the spin-flipped ECT probabilities are

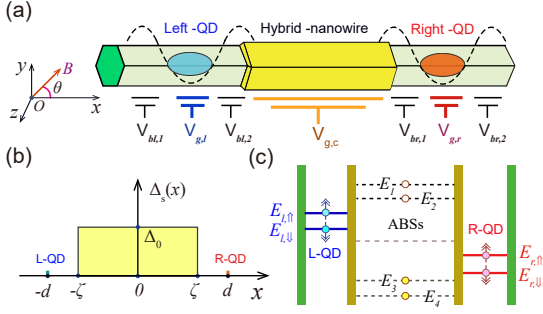


FIG. 1. (a) Schematic diagram of two distant gate-defined QDs in a semiconductor nanowire with the connection section proximitized by a s -wave superconductor, in which $V_{bl(r),1}$ and $V_{bl(r),2}$ represent the two barrier-gate potentials for the left (right) QD, and $V_{g,l(r)}$ and $V_{g,c}$ correspond to the respective plunger gate potentials. The inset depicts the direction of an applied magnetic field, i.e., $\mathbf{B} = B(\cos\theta, \sin\theta, 0)$. (b) The variation of the proximity-induced superconducting gap Δ_s along the wire-axis (x) direction, in which 2ζ characterizes the length of the proximitized section and $2d$ the interdot distance. (c) The low-energy level structures of the two-sided QDs and middle hybrid nanowire, with $E_{l(r),\uparrow}$ and $E_{l(r),\downarrow}$ indicating the two localized Zeeman-splitting states of the left (right) QD and $E_{j=1-4}$ the centered four Andreev bound states (ABSs).

also observed in the presence of a parallel magnetic field. Interestingly, our model allows us to extract the effective average on-site energy based on the observed gate-tuning asymmetry. Furthermore, we predict that, under the effect of the ECT and CAR incorporating the QD states tuning, an anisotropic superexchange interaction naturally emerges between the separated electrons confined in two QDs in the strong Coulomb-blockade regime.

Model—The two separated QDs we consider are defined around the two ends of a semiconductor nanowire with strong Rashba SOI, e.g., InAs or InSb nanowire, with the connection section proximitized by a superconductor Al, as shown in Fig. 1(a). In the presence of a magnetic field $\mathbf{B} = B(\cos\theta, \sin\theta, 0)$ applied in the $x-y$ plane, the single-particle Hamiltonian of the hybrid nanowire along the x -axial direction reads as

$$H_e(x) = -\frac{\hbar^2}{2} \frac{\partial}{\partial x} \frac{1}{m_e(x)} \frac{\partial}{\partial x} + \frac{g(x)\mu_B}{2} \mathbf{B} \cdot \boldsymbol{\sigma} + V(x) - i\frac{\hbar}{2} \left[\frac{\partial}{\partial x} \alpha(x) + \alpha(x) \frac{\partial}{\partial x} \right] \sigma_y, \quad (1)$$

where $m_e(x)$, $g(x)$, and $\alpha(x)$ respectively correspond to the site-dependent electron effective mass (EMS), the Landé- g factor, and the Rashba SOI strength absorbing the partial metallization effect caused by the coated superconductor. $\boldsymbol{\sigma} = (\sigma_x, \sigma_y, \sigma_z)$ denotes the Pauli matrix-vector, μ_B is the Born magneton, and $V(x)$ depicts the confinement potential induced by the gate voltages. In addition, nonzero proximity-induced supercon-

ductivity can emerge in the middle section as $\Delta_s(x) = \Delta_0 \Theta(|x| - \zeta)$, with Δ_0 representing the induced superconducting gap, $\Theta(x)$ being a Heaviside function, and ζ the half-width of the proximitized section [see Fig. 1(b)]. **Localized confined states**—Without loss of generality, the local confinement potential of the left/right QD can be modeled as $V_{l/r}(x) = m_{e,0}\omega_0^2(x \pm d)^2/2 + V_{g,l/r}$, in which $m_{e,0/1}$ ($\alpha_{0/1}$ and $g_{0/1}$) quantifies the specific value of the EMS (the SOI strength and Landé factor) in the bare/proximitized nanowire, ω_0 is the frequency of the harmonic potential, d is the half interdot distance, and $V_{g,l/r}$ the relevant plunger-gate potential. In the case of $\Delta_{z,0} \equiv g_0\mu_B B \ll \hbar\omega_0$, the lowest Zeeman-splitting states of the QDs are approximated as

$$\begin{aligned} |\Psi_{l/r,\uparrow}\rangle &= \phi_0(x \pm d) \left[ie^{-i\frac{x \pm d}{x_{so}}} \cos\frac{\vartheta}{2} |\uparrow\rangle + e^{i\frac{x \pm d}{x_{so}}} \sin\frac{\vartheta}{2} |\downarrow\rangle \right] \\ |\Psi_{l/r,\downarrow}\rangle &= \phi_0(x \pm d) \left[ie^{-i\frac{x \pm d}{x_{so}}} \sin\frac{\vartheta}{2} |\uparrow\rangle - e^{i\frac{x \pm d}{x_{so}}} \cos\frac{\vartheta}{2} |\downarrow\rangle \right], \end{aligned} \quad (2)$$

where $\phi_0(x) = (\sqrt{\pi}x_0)^{-1/2} \exp[-x^2/(2x_0^2)]$ is the electron spatial wave-function with $x_0 = [\hbar/(m_{e,0}\omega_0)]^{1/2}$ and the effective spin-orbit length $x_{so} = \hbar/(m_{e,0}\alpha_0)$. Here, $\vartheta = \arccos[\sin\theta/f(\theta)]$ characterizes the spin mixing induced by SOI with $f(\theta) = (\sin^2\theta + e^{-2x_0^2/x_{so}^2} \cos^2\theta)^{1/2}$, and $|\uparrow\rangle$ and $|\downarrow\rangle$ represent the spin-polarized states with $\sigma_y|\uparrow\rangle = |\uparrow\rangle$ and $\sigma_y|\downarrow\rangle = -|\downarrow\rangle$, respectively. Correspondingly, the energies of the quasi-spin states read as $E_{\nu,\uparrow/\downarrow} = E_\nu \pm f(\theta)\Delta_{z,0}/2$, with $\nu = l, r$ and $E_\nu = V_{g,\nu} + (\hbar\omega_0 - m_{e,0}\alpha_0^2)/2$ the effective orbital on-site energies.

For the intermediate proximitized nanowire, the combination of the plunger-gate potential $V_{g,c}$ and the two inner barrier-gate potentials of the QDs [see $V_{bl,2}$ and $V_{br,1}$ in Fig. 1(a)], in principle, can also endow a concave-shaped confinement, $V_{in}(x) = m_{e,1}\omega_1^2 x^2/2 + V_{g,c}$ with ω_1 specifying the parabolic potential. Then, the effective Bogoliubov-de Gennes (BdG) Hamiltonian for the proximities section can be expressed as $H_{\text{BdG}} = [p_x^2/(2m_{e,1}) + \alpha_1 p_x \sigma_y + V_{in}(x)]\tau_z + \Delta_0 \tau_x + \Delta_{z,1}(\cos\theta \sigma_x + \sin\theta \sigma_y)/2$, with $p_x = -i\hbar\partial/(\partial x)$, $\Delta_{z,1} = g_1\mu_B B$, and $\tau_{x,y,z}$ the Pauli matrices defining in the particle-hole (PH) space. As such, the low-energy ABSs of the intermediate nanowire can be analytically derived based on the effective Hamiltonian [42]. The energies of the lowest two ABSs above the Fermi (zero-energy) level take the form of

$$E_{1/2} = \sqrt{\mu^2 + \Delta_0^2} \pm \frac{f_1(\theta)}{2} \Delta_{z,c}, \quad (3)$$

with $\mu = V_{g,c} + (\hbar\omega_1 - m_{e,1}\alpha_1^2)/2$ and $f_1(\theta)$ similar to $f(\theta)$ but with x_0 and x_{so} replaced by $x_1 = [\hbar/(m_{e,1}\omega_1)]^{1/2}$ and $x'_{so} = \hbar/(m_{e,1}\alpha_1)$, respectively. The energies of the nearest two ABSs below the Fermi level [as seen

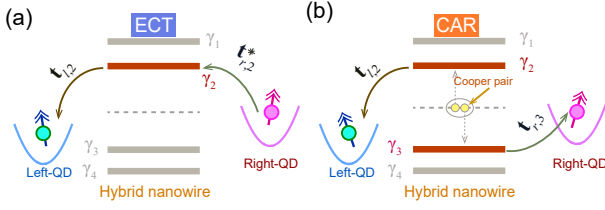


FIG. 2. (a) Schematic diagram of an ECT, in which there is an electron quasi-spin state transferring from the right-QD to the left-QD as mediated by the ABS γ_2 of the middle hybrid nanowire. (b) Schematic of a CAR with two electron quasi-spin states creating in the two-sided QDs, and under the intermediation of two middle PH-symmetric ABSs, i.e., γ_2 and γ_3 . Here, $\mathbf{t}_{l(r),j}$ indicate the direct tunnel-coupling amplitude vector between the left (right) QD states and the ABS γ_j , and is comprised by $\mathbf{t}_{l(r),j} = \{t_{l(r)\uparrow,j}, t_{l(r)\downarrow,j}\}$.

in Fig. 1(c)] are given by $E_{3/4} = -E_{2/1}$, in accordance with the PH symmetry of the BdG Hamiltonian $\mathcal{P}H_{\text{BdG}}\mathcal{P}^{-1} = -H_{\text{BdG}}$, with $\mathcal{P} = i\tau_y\sigma_yK$ and K being the PH and complex-conjugation operators, respectively. Due to the coexistence of the SOI and the proximity effect, they represent quasi-particles as a combination of electron and hole components characterized by different spin mixings. Hereafter, they are denoted by the Bogoliubov quasi-particle operators γ_j with $j = 1 - 4$ respectively.

The extension of the ABSs in the bare section leads to direct tunnel-couplings with the QD states as defined in Eq. (2). Let's denote the creation (annihilation) operator for the quasi-spin state $|\Psi_{l/r,s}\rangle$ with $s = \uparrow, \downarrow$ as $d_{l/rs}^\dagger$ ($d_{l/rs}$), then the corresponding tight-binding (TB) Hamiltonian for the hybrid nanostructure can be formulated as

$$H_{\text{TB}} = \sum_{\nu,s} E_{\nu,s} d_{\nu,s}^\dagger d_{\nu,s} + \sum_j E_j \gamma_j^\dagger \gamma_j + \sum_{\nu,s,j} (t_{\nu,s,j} d_{\nu,s}^\dagger \gamma_j + \text{h.c.}), \quad (4)$$

in which $t_{\nu,s,j}$ characterizes the tunnel-coupling amplitude from the QD state $|\Psi_{\nu,s}\rangle$ to the ABS γ_j . Specifically, in addition to a structure-dependent (spinless) parameter t_0 , because of SOI, $t_{\nu,s,j}$ also depends on the degrees of spin mixing in the two localized states and the accumulated spin rotation phase $\Phi_{\text{so}} = \tilde{d}/x_{\text{so}}$ in the tunneling. Note that, the effective length \tilde{d} is different from the interdot distance d , due to the SOI inhomogeneity along the axial direction. The details of the direct tunneling amplitude $t_{\nu,s,j}$ are presented in the Supplementary [42]. **Effective interdot interactions**— When the QD states are largely detuned from the ABSs, i.e., $E_{\nu,s} \ll |E_j|$, it is interesting to find that the direct tunnel-couplings in Eq. (4) can simultaneously facilitate the interdot elastic-cotunneling (ECT) and crossed Andreev

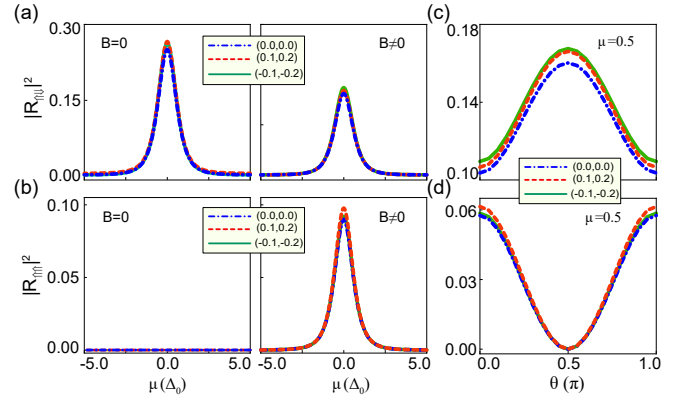


FIG. 3. (a) The absolute values of the spin-flipped CAR amplitude $|R_{\uparrow\downarrow}|^2$, in units of $4t_0^4/\Delta_0^2$, as a function of μ with different on-site energies E_l and E_r (see the inset), and $\theta = 0$. The right (left) panel corresponds to the case with a zero (nonzero) magnetic field. (b) Same as (a), but show the trends of the spin-conserved quantity $|R_{\uparrow\uparrow}|^2$ in different conditions. (c) and (d) At a fixed μ , the variations $|R_{\uparrow\downarrow}|^2$ and $|R_{\uparrow\uparrow}|^2$ versus θ in the presence of the magnetic field and with different on-site energies. Here, the energies E_l , E_r , and the chemical potential μ are in units of Δ_0 , the nonzero magnetic field is characterized by $\tilde{\Delta}_{z,0} = 0.1\Delta_0$, and the other parameters are fixed as $\tilde{d} = 200$ nm, $x_{\text{so}} = 160$ nm, $x'_{\text{so}} = 240$ nm, $x_0 = 30$ nm, $x_1 = 70$ nm, and $\Delta_{z,c} = 0.5\Delta_{z,0}$ in the simulations.

reflection (CAR). Practically, this is accompanied by virtual excitations or evacuations of the middle higher- or lower-energy ABSs, as seen in Fig. 2. Through using the Schrieffer-Wolff transformation to eliminate the intermediate processes, the effective Hamiltonian for the two long-range interactions can be found as $H_{\text{ECT}} = \sum_{ss'=\uparrow,\downarrow} (d_{ls}^\dagger T_{ss'} d_{rs'} + \text{h.c.})$ and $H_{\text{CAR}} = \sum_{ss'} (d_{ls}^\dagger R_{ss'} d_{rs'}^\dagger + \text{h.c.})$, with the spin-dependent amplitudes evaluated by

$$T_{ss'} = \sum_{j=1-4} \frac{t_{ls,j} t_{rs',j}^*}{2} \left(\frac{1}{E_{l,s} - E_j} + \frac{1}{E_{r,s'} - E_j} \right)$$

$$R_{ss'} = \sum_{j=1-4} \frac{t_{ls,j} t_{rs',(5-j)}}{2} \left(\frac{1}{E_{l,s} - E_j} + \frac{1}{E_{(5-j)} - E_{r,s'}} \right). \quad (5)$$

Intuitively, as can be seen above, ECT is achieved via the sequential single-electron (γ_j) transports. In contrast, CAR involves the creation or annihilation of two electrons in the QDs, mediated by the PH-symmetric ABSs γ_j and γ_{5-j} originating from a Cooper pair [see Fig. 2(b)]. We want to stress that, the explicit expressions of $t_{\nu,s,j}$ and $E_{\nu,s}$ are all obtainable in our model, hence allowing the study of the CARs and ECTs in a complete sense. In what follows, we discuss this in more detail.

By noting the energy conservation warranted by the paired ABSs in $R_{ss'}$, i.e., $E_j + E_{5-j} \equiv 0$, the Hamiltonian

for the CAR interaction can be effectively formulated as

$$H_{\text{CAR}} = -\frac{t_0^2 \Delta_0}{\mu^2 + \Delta_0^2} \begin{pmatrix} d_{l\downarrow} \\ -d_{l\uparrow} \end{pmatrix}^\dagger \hat{\mathbf{U}}(2\Phi_{\text{so}}) \begin{pmatrix} d_{r\uparrow}^\dagger \\ d_{r\downarrow}^\dagger \end{pmatrix} + \text{h.c.}, \quad (6)$$

with $\hat{\mathbf{U}}(2\Phi_{\text{so}}) = \exp[-2i\Phi_{\text{so}}\hat{n} \cdot \boldsymbol{\sigma}]$ representing the spin rotation matrix induced by SOI and $\hat{n} = (\sin\vartheta, 0, \cos\vartheta)$ the direction vector the rotation axis. In this form, the μ -dependence of the amplitude $R_{ss'}$ is thus directly revealed by the coefficient of Eq. (6) now. Despite of the values of E_ν and B , as shown in Fig. 3(a), $|R_{s\bar{s}}|^2$ manifests a rather robust dependency of μ , i.e., decreasing with increasing $|\mu|$, and always attain its maximum at $\mu = 0$. On the other hand, Fig. 3(c) shows the dependence on the specific expression of \hat{n} , where robustness against the on-site energies of the QD states ($E_{l,r}$) can also be observed. Similar results for $|R_{ss}|^2$ are plotted in Figure 3(b, d), except at $B = 0$ or $\theta = \pm\pi/2$ where the spin-conserved CAR is suppressed because of the spin conservation. Note that the above equation is explicitly independent of the on-site energy of the QD states; therefore, for CARs, the main features are reserved even without involving the effects of the QD states. This explains why the model utilized in Ref. [41] is sufficient to interpret the observed CARs in experiments, which, however, is definitely not for the ECTs, as shown following.

Similarly, $T_{ss'}$ for ECT is further reformulated as,

$$T_{ss'} = -\frac{t_0^2(\mu + E_{ss'})}{\mu^2 + \Delta_0^2} \left[\hat{\mathbf{U}}(-2\Phi_{\text{so}}) \right]_{ss'} + \frac{t_0^2 \Delta_{z,c} f_1(\theta)}{2(\mu^2 + \Delta_0^2)} \times \left\{ [\boldsymbol{\Pi}(\theta) \cdot \boldsymbol{\sigma}]_{ss'} + i\delta_{ss'} \sin(2\Phi_{\text{so}}) \cos\varphi \right\}, \quad (7)$$

with $E_{ss'} = (E_{l,s} + E_{r,s'})/2$, $\delta_{ss'}$ being the Kronecker delta function, $\varphi = \arccos[\sin\theta/f_1(\theta)]$, and $\boldsymbol{\Pi}(\theta)$ is a parameter vector [42].

Admitted by the spin conservation with $B = 0$, the spin-flipped ECTs are forbidden and hence we have $T_{s\bar{s}} = 0$, as shown in Fig. 4(a). Contrarily, the spin-conserved quantity $|T_{ss}|^2$ exhibit evident μ - and $E_{l,r}$ -dependencies, as can be seen from Fig. 4(b). It is found $|T_{ss}|^2$ vanishes at $\mu \simeq -E_{ss}$, accompanied with two local peaks emerging around. Interestingly, based on Eq. (7), the ratio between these two peak values can be evaluated as $\gamma_0 = [E_{ss} + (E_{ss}^2 + \Delta_0^2)^{1/2}]^2 / [E_{ss} - (E_{ss}^2 + \Delta_0^2)^{1/2}]^2$. As a result, the spin-conserved tunneling probability is generically μ -asymmetric. This, remarkably, can well capture the experimental observations in Ref. 39 [see Fig. 2(f) therein], according to which estimations of $\gamma_0 \simeq 2.4$ and the average on-site energies $E_{ss} \simeq 0.22\Delta_0$ can thus be extracted. We want to emphasize that, the above significant prediction we found for the spin-conserved ECT has not been discussed anywhere yet, which we believe is ascribed to the inclusion of the nonzero on-site energies considered in our model.

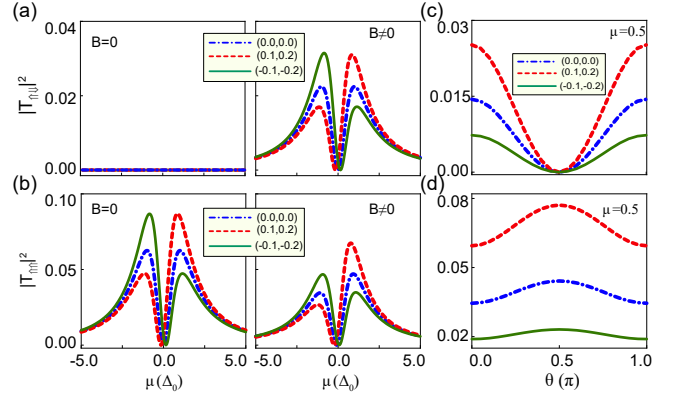


FIG. 4. (a)-(b) The absolute values of the spin-dependent ECT amplitudes between the double QDs in Fig. 3, $|T_{\uparrow\downarrow}|^2$ and $|T_{\uparrow\uparrow}|^2$, in units of $4t_0^2/\Delta_0^2$, as a function of μ , with different on-site energies (E_l and E_r) and magnetic-field strength (B), and the direction angle $\theta = 0$. (c)-(d) The variations of $|T_{\uparrow\downarrow}|^2$ and $|T_{\uparrow\uparrow}|^2$ versus θ , in the case of different on-site energies and with $\Delta_{z,0} = 0.1\Delta_0$ and $\mu = 0.5\Delta_0$.

Note that, the asymmetric μ -dependence of $|T_{ss}|^2$ can also appear when a parallel magnetic field ($B \neq 0$) is applied, even when $E_{ss} = 0$, see the blue dashed line in Fig. 4(b). Similarly, spin-flipped ECT comes to play in the presence of $B \neq 0$ as well, presenting a much similar μ -dependence as that for $|T_{ss}|^2$ at $B = 0$ [right panel, Fig. 4(a)]. This again, when considering $E_{s\bar{s}} \neq 0$, can well explain what has been observed for $T_{s\bar{s}}$ in the experiment, see Fig. 3(d) of Ref. [39]. Moreover, the spin-dependent ECT amplitudes also vary with the direction of the magnetic field. As shown in Figs. 4(c, d), for the case of $\mu > E_{\nu,s}$, $|T_{s\bar{s}}|^2$ and $|T_{ss}|^2$ attain their local maximum and minimum values at $\theta = 0, \pi$, respectively, showing a significant modulation by the on-site energies.

More physics relates to on-site energy— As has been addressed in Ref. [32], the formation of poor man's MBSs demands double QDs with symmetric on-site energy and with the low-energy Zeeman splitting states kept around the Fermi level, i.e., $E_{\nu,\downarrow} \simeq 0$. Being a zero-energy and half-fermion state, the emergence of a pair of the MBSs can also be manifested by the parity degeneracy in the ground state of the double QDs. Figure 5(a) shows the distribution of the parity of the ground state in the $\theta - \mu$ plane, where, for completeness, the effect of intradot Coulomb repulsions is also included in the calculation [42]. Clearly, the boundary between the odd-parity and even-parity areas indicates the correlation of the two modulation parameters required to attain the parity degeneracy. This is consistent with the conventional criteria for the poor man's MBSs in Ref. [31], where a balance between the interdot spin-conserved ECT and CAR $|T_{\downarrow\downarrow}|^2 = |R_{\downarrow\downarrow}|^2$ is necessary. Note that, as there is no spin-conserved CAR at $\theta = \pi/2$ (see Fig. 3(d)), the emergence of parity degeneracy does not really ensure

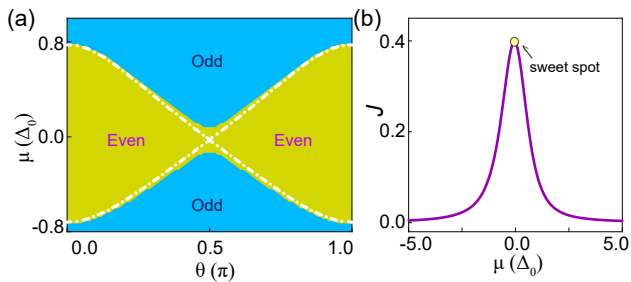


FIG. 5. (color online) (a) The parity-phase diagram of the ground state of the double QDs in the $\theta - \mu$ plane, with $E_{l,r\downarrow} = 0$, $\Delta_{z,0} = 0.2$, $U = 5.0$ (in a units of Δ_0) and the other system parameters as same as that in Fig. 3. In addition, the dot-dashed (white) curves indicate the correlation of the two modulation parameters to attain $|T_{\downarrow\downarrow}|^2 = |R_{\downarrow\downarrow}|^2$. (b) Within the strong Coulomb-blockade regime of $E_l = -0.3$, $E_r = -0.4$, and $\Delta_{z,0} = 0.05$, the superexchange interaction strength J in Eq. (8), in a unit of $4t_0^4/\Delta_0^2$, as a function of μ .

the creation of the MBSs, as indicated by the deviation emerging there in Fig. 5(a).

When tuned into the strong Coulomb blockade regime, i.e., $|E_{\nu,s}|, |E_j| \ll U$ with U denoting the intradot Coulomb repulsion strength, the electron occupancy of the double QDs is fixed as (1,1), i.e., each dot is now occupied by a single electron. In this scenario, the electrons of the two QDs will establish an effective exchange interaction via the interdot CAR and ECT, as given in Eqs. (6) and (7). Explicitly, at the limit of $|E_{\nu}/\Delta_{z,s}| \gg 1$, the superexchange Hamiltonian is found as, $\mathcal{H}_{\text{eff}} = J \left[\cos^2(2\Phi_{\text{so}}) \mathbf{S}_l \cdot \mathbf{S}_r + \sin(4\Phi_{\text{so}}) \hat{n} \cdot (\mathbf{S}_l \times \mathbf{S}_r) + \sin^2(2\Phi_{\text{so}}) \mathbf{S}_l \overleftrightarrow{\Gamma} \mathbf{S}_r \right]$ [42]. Here, we have $\overleftrightarrow{\Gamma} = 2\hat{n}\hat{n} - 1$, $\mathbf{S}_{\nu=l,r} = (1/2) \sum_{s,s'} d_{\nu s'}^\dagger \boldsymbol{\sigma}_{s's} d_{\nu s}$ representing the electron quasi-spin operators, and the strength of the exchange interaction

$$J = \frac{t_0^4 U}{(\mu^2 + \Delta_0^2)^2} \left[\frac{(2\mu + E_+)^2}{U^2 - E_-^2} - \frac{4\Delta_0^2}{E_+(2U + E_+)} \right], \quad (8)$$

with $E_{\pm} = E_l \pm E_r$. It is evident that the direction of the Dzyaloshinskii-Moriya vector in \mathcal{H}_{eff} , viz., \hat{n} , vary with the direction of the magnetic field. Moreover, the exchange strength J can be regulated by the chemical potential μ , as shown in Fig. 5(b). When μ is tuned approaching to (away from) the zero point, J is effectively switched on (off). Specifically, at $\mu = 0$, it is found that the maximum of J is achieved and the modulation of the exchange interaction reaches a sweet point as $\partial J/\partial \mu = 0$. We believe this is important in studying the long-range spin transfer and exchange gate using the QD-coupled superconducting nanostructures.

Conclusion— Focusing on the interaction between two separated QDs mediated by the ABSs of a superconducting proximitized nanowire, we clarify different interesting effects on the interdot ECTs and CARs from tuning the

on-site energies of the QD states, as explicitly considered in our model. Regarding the CARs, we demonstrate that the applied modulations do not affect the spin-dependent tunneling amplitudes. This validates the sufficiency of the simplified treatment in Ref. [41], in which the specific on-site energies of the QD states are not accounted for. However, the lack of interpretation of the μ -asymmetry for ECTs, as observed in the experiment [39], immediately demands a theoretical model going beyond that used in Ref. [41].

Instead, the complete TB model considered in this work can correctly capture all the experimental observations [39]. Besides the predictions of those μ -asymmetry for ECTs with or without the magnetic field (as mentioned above), within our scheme, average on-site energy can be effectively extracted according to the experimental observations [39]. We further demonstrate that our model allows for exploring some other intriguing phenomena, such as the poor man's MBSs via a parity phase diagram and a controllable anisotropic superexchange interaction between electrons. Therefore, we believe our work will facilitate more interesting studies of the rich physics in this system.

Acknowledgment.— We thank for useful discussion with D. Loss, L. Kouwenhoven, Y. Zhou, J-Y Wang, and P. Zhang. This work is supported by the National Natural Science Foundation of China (Grants No. 92165208 and No. 11874071). C. Z. acknowledges support from NSFC (Grant No. 12104043).

* liuzh@baqis.ac.cn
 † zengcc@baqis.ac.cn
 ‡ hqxu@pku.edu.cn

- [1] Guido Burkard, Michael J. Gullans, Xiao Mi, and Jason R. Petta, Superconductor-Csemiconductor hybrid-circuit quantum electrodynamics, *Nat. Rev. Phys.* **2**, 129-140 (2020).
- [2] Karsten Flensberg, Felix von Oppen, and Ady Stern, Engineered platforms for topological superconductivity and Majorana zero modes, *Nat. Rev. Mater.* **6**, 944-958 (2021).
- [3] S. M. Frolov, M. J. Manfra, and J. D. Sau, Topological superconductivity in hybrid devices, *Nat. Phys.* **16**, 718-724 (2020).
- [4] R. M. Lutchyn, E. P. A. M. Bakkers, L. P. Kouwenhoven, P. Krogstrup, C. M. Marcus, and Y. Oreg, Majorana zero modes in superconductor-Csemiconductor heterostructures, *Nat. Rev. Mater.* **3**, 52-68 (2018).
- [5] A. Zazunov, R. Egger, T. Jonckheere, and T. Martin, Anomalous Josephson Current through a Spin-Orbit Coupled Quantum Dot, *Phys. Rev. Lett.* **103**, 147004 (2009).
- [6] Eric M. Spanton, Mingtang Deng, Saulius Vaitiekėnas, Peter Krogstrup, Jesper Nygård, Charles M. Marcus, and Kathryn A. Moler, Current-phase relations of few-mode InAs nanowire Josephson junctions, *Nat. Phys.* **13**, 1177-

- 1181 (2017).
- [7] D. B. Szombati, S. Nadj-Perge, D. Car, S. R. Plissard, E. P. A. M. Bakkers, and L. P. Kouwenhoven, Josephson ϕ_0 -junction in nanowire quantum dots, *Nat. Phys.* **12**, 568-572 (2016).
- [8] D. Laroche, D. Bouman, D. J. van Woerkom, A. Proutski, C. Murthy, D. I. Pikulin, C. Nayak, Ruben J. J. van Gulik, Jesper Nygård, Peter Krogstrup, Leo P. Kouwenhoven, and Attila Geresdi, Observation of the 4π -periodic Josephson effect in indium arsenide nanowires, *Nat. Commun.* **10**, 245 (2019).
- [9] Muhammad Nadeem, Michael S. Fuhrer, and Xiaolin Wang, The superconducting diode effect, *Nat. Rev. Phys.* **5**, 558-577 (2023).
- [10] Henry F. Legg, Daniel Loss, and Jelena Klinovaja, Superconducting diode effect due to magnetochiral anisotropy in topological insulators and Rashba nanowires, *Phys. Rev. B* **106**, 104501 (2022).
- [11] Tomohiro Yokoyama, Mikio Eto, and Yuli V. Nazarov, Anomalous Josephson effect induced by spin-orbit interaction and Zeeman effect in semiconductor nanowires, *Phys. Rev. B* **89**, 195407 (2014).
- [12] Haitian Su, Ji-Yin Wang, Han Gao, Yi Luo, Shili Yan, Xingjun Wu, Guoan Li, Jie Shen, Li Lu, Dong Pan, Jianhua Zhao, Po Zhang, and H. Q. Xu, Microwave-assisted unidirectional superconductivity in Al-InAs nanowire-Al junctions under magnetic fields, [arXiv:2402.02137](https://arxiv.org/abs/2402.02137).
- [13] R. M. Lutchyn, J. D. Sau, and S. Das Sarma, Majorana Fermions and a topological phase transition in semiconductor-superconductor heterostructures, *Phys. Rev. Lett.* **105**, 077001 (2010).
- [14] Y. Oreg, G. Refael, and F. von Oppen, Helical liquids and Majorana bound states in quantum wires, *Phys. Rev. Lett.* **105**, 177002 (2010).
- [15] Microsoft Azure Quantum, Interferometric Single-Shot Parity Measurement in an InAs-Al Hybrid Device, [arXiv:2401.09549](https://arxiv.org/abs/2401.09549)
- [16] M. Hays, V. Fatemi, D. Bouman, J. Cerrillo, S. Diamond, K. Serniak, T. Connolly, P. Krogstrup, J. Nygård, A. Levy Yeyati, A. Geresdi, M. H. Devoret, Coherent manipulation of an Andreev spin qubit, *Science* **373**, 430-433 (2021).
- [17] C. Padurariu and Yu. V. Nazarov, Theoretical proposal for superconducting spin qubits, *Phys. Rev. B* **81**, 144519 (2010).
- [18] M. Pita-Vidal, A. Bargerbos, R. Zitko, L. J. Splitthoff, L. Grunhaupt, J. J. Wesdorp, Y. Liu, L. P. Kouwenhoven, R. Aguado, B. van Heck, A. Kou, and C. K. Andersen, Direct manipulation of a superconducting spin qubit strongly coupled to a transmon qubit, *Nat. Phys.* **19**, 1110-1115 (2023)
- [19] A. P. Higginbotham, S. M. Albrecht, G. Kirsanskas, W. Chang, F. Kueemeth, P. Krogstrup, T. S. Jespersen, J. Nygård, K. Flensberg, and C. M. Marcus, Parity lifetime of bound states in a proximitized semiconductor nanowire, *Nat. Phys.* **11**, 1017-1021 (2015).
- [20] T.W. Larsen, K. D. Petersson, F. Kueemeth, T. S. Jespersen, P. Krogstrup, J. Nygård, and C. M. Marcus, Semiconductor-Nanowire-Based Superconducting Qubit, *Phys. Rev. Lett.* **115**, 127001 (2015).
- [21] M. Spethmann, S. Bosco, A. Hofmann, J. Klinovaja, D. Loss, High-fidelity two-qubit gates of hybrid superconducting-semiconducting singlet-triplet qubits, [arXiv:2304.05086](https://arxiv.org/abs/2304.05086).
- [22] M. Spethmann, X.-P. Zhang, J. Klinovaja, and D. Loss, Coupled superconducting spin qubits with spin-orbit interaction, *Phys. Rev. B* **106**, 115411 (2022).
- [23] Mahn-Soo Choi, C. Bruder, and Daniel Loss, Spin-dependent Josephson current through double quantum dots and measurement of entangled electron states, *Phys. Rev. B* **62**, 13569 (2000).
- [24] R. S. Deacon, A. Oiwa, J. Sailer, S. Baba, Y. Kanai, K. Shibata, K. Hirakawa, and S. Tarucha, Cooper pair splitting in parallel quantum dot Josephson junctions, *Nat. Commun.* **6**, 7446 (2015).
- [25] Q. Wang, S. L. D. ten Haaf, I. Kulesh, D. Xiao, C. Thomas, M. J. Manfra, and S. Goswami, Triplet correlations in Cooper pair splitters realized in a two-dimensional electron gas, *Nat. Commun.* **14**, 4876 (2023).
- [26] G. Wang, T. Dvir, G. P. Mazur, C.-X. Liu, N. van Loo, S. L. D. ten Haaf, A. Bordin, S. Gazibegovic, G. Badawy, E. P. A. M. Bakkers, M. Wimmer, and L. P. Kouwenhoven, Singlet and triplet Cooper pair splitting in hybrid superconducting nanowires, *Nature* **612**, 448-453 (2022).
- [27] O. Kürtössy, Z. Scherübl, G. Fülöp, I. E. Lukács, T. Kanne, J. Nygård, P. Makk, and S. Csonka, Parallel InAs nanowires for Cooper pair splitters with Coulomb repulsion, *npj Quantum Mater.* **7**, 88 (2022).
- [28] F. Brange, K. Prech, and C. Flindt, Dynamic Cooper Pair Splitter, *Phys. Rev. Lett.* **127**, 237701 (2021).
- [29] A. Bordoloi, V. Zannier, L. Sorba, C. Schönenberger, and A. Baumgartner, Spin cross-correlation experiments in an electron entangler, *Nature* **612**, 454-458 (2022).
- [30] Jay D. Sau and S. Das Sarma, Realizing a robust practical Majorana chain in a quantum-dot-superconductor linear array, *Nat. Commun.* **3**, 964 (2012).
- [31] M. Leijnse and K. Flensberg, Parity qubits and poor man's Majorana bound states in double quantum dots, *Phys. Rev. B* **86**, 134528 (2012).
- [32] A. Tsintzis, R. Seoane Souto, and M. Leijnse, Creating and detecting poor man's Majorana bound states in interacting quantum dots, *Phys. Rev. B* **106**, L201404 (2022).
- [33] C.-X. Liu, H. Pan, F. Setiawan, M. Wimmer, and J. D. Sau, Fusion protocol for Majorana modes in coupled quantum dots, *Phys. Rev. B* **108**, 085437 (2023).
- [34] A. Tsintzis, R. S. Souto, K. Flensberg, J. Danon, and M. Leijnse, Roadmap towards Majorana qubits and non-abelian physics in quantum dot-based minimal Kitaev chains, [arXiv:2306.16289](https://arxiv.org/abs/2306.16289).
- [35] W. Samuelson, V. Svensson, and M. Leijnse, Minimal quantum dot based Kitaev chain with only local superconducting proximity effect, *Phys. Rev. B* **109**, 035415 (2024).
- [36] R. S. Souto, A. Tsintzis, M. Leijnse, and Jeroen Danon, Probing Majorana localization in minimal Kitaev chains through a quantum dot, *Phys. Rev. Research* **5**, 043182 (2023).
- [37] T. Dvir, G. Wang, N. van Loo, C.-X. Liu, G. P. Mazur, A. Bordin, S. L. D. ten Haaf, J.-Y. Wang, D. van Driel, F. Zatelli, X. Li, F. K. Malinowski, S. Gazibegovic, G. Badawy, E. P. A. M. Bakkers, M. Wimmer, and L. P. Kouwenhoven, Realization of a minimal Kitaev chain in coupled quantum dots, *Nature* **614**, 445-450 (2023).
- [38] A. Bordin, C.-X. Liu, T. Dvir, F. Zatelli, S. L. D. ten Haaf, D. van Driel, G. Wang, N. van Loo, T. van Caekenberghe, J. C. Wolff, Y. Zhang, G. Badawy, S. Gazibegovic, E. P. A. M. Bakkers, M. Wimmer, L. P.

- Kouwenhoven, and G. P. Mazur, Signatures of Majorana protection in a three-site Kitaev chain, [arXiv:2402.19382](https://arxiv.org/abs/2402.19382).
- [39] A. Bordin, G. Wang, C.-X. Liu, S. L. D. ten Haaf, N. van Loo, G. P. Mazur, D. Xu, D. van Driel, F. Zatelli, S. Gazibegovic, G. Badawy, E. P. A. M. Bakkers, M. Wimmer, L. P. Kouwenhoven, and T. Dvir, Tunable Crossed Andreev Reflection and Elastic Cotunneling in Hybrid Nanowires, *Phys. Rev. X* **13**, 031031 (2023).
- [40] A. Bordin, X. Li, D. van Driel, J. C. Wolff, Q. Wang, S. L. D. ten Haaf, G. Wang, N. van Loo, L. P. Kouwenhoven, and T. Dvir, Crossed Andreev Reflection and Elastic Cotunneling in Three Quantum Dots Coupled by Superconductors, *Phys. Rev. Lett.* **132**, 056602 (2024).
- [41] C.-X. Liu, G. Wang, T. Dvir, and M. Wimmer, Tunable Superconducting Coupling of Quantum Dots via Andreev Bound States in Semiconductor-Superconductor Nanowires, *Phys. Rev. Lett.* **129**, 267701 (2022).
- [42] See Supplemental Material at [URL will be inserted by publisher] for details of the Andreev bound states of the middle hybrid nanowire and the direct tunnel-coupling amplitudes $t_{\nu s, j}$, the spin-dependent interdot ECT and CAR amplitudes $T_{ss'}$ and $R_{ss'}$, as well as derivations of the parity-phase diagram of the ground state of the double QDs in Fig. 5(a) and the superexchange interaction Hamiltonian \mathcal{H}_{eff} for the QDs in the strong Coloumb-blockade regime.